Electronic Supplementary Information (ESI)

In situ magnetic and electronic investigation of the early stage oxidation of Fe nanoparticles using x-ray photo-emission electron microscopy

C. A. F. Vaz,[a] A. Balan,[a] F. Nolting[a] and A. Kleibert[a]

[a]Swiss Light Source, Paul Scherrer Institut, Villigen PSI, 5232 Switzerland.

*corresponding author: armin.kleibert@psi.ch

In this document, we provide additional information (i) on the structural characterization of the Fe nanoparticles and (ii) on the model calculations carried out to deconvolute the x-ray absorption spectra of the partially oxidized Fe nanoparticles.

(i) Size and shape characterization of iron nanoparticles

After the *in situ* magnetic and spectroscopic investigation using photoemission electron microscopy (PEEM), the particles are characterized *ex situ* by means of complementary microscopy. The goal is to identify particles that are well separated and which have a regular shape. This cannot be achieved with X-ray PEEM, which has a spatial resolution of the order of 50 - 100 nm. For identification of the very same particles, we make use of lithographically defined gold/chromium markers that were fabricated on the Si substrate prior to the Fe nanoparticle deposition.[1] To determine the particle shape, we use scanning electron microscopy, SEM, (Zeiss Supra VP55), which has lateral spatial resolution down to the nanometer range, while to determine the particle size we use atomic force microscopy, AFM, (Nanoscope DI 3100), which provides an accurate height profile resolution,[3] used here in tapping mode using a standard Si tip (μmasch HQ:NSC15/Al BS). Representative results for the images obtained from the different techniques covering the same region in the sample, are given in Fig. S1. After identification of isolated nanoparticles in large area SEM scans, SEM images similar to those shown in Fig.1b and Fig. S1b (insets), and AFM scans similar to those shown in Fig, S1c, were carried in order to accurate determine the shape and size of each individual particle.

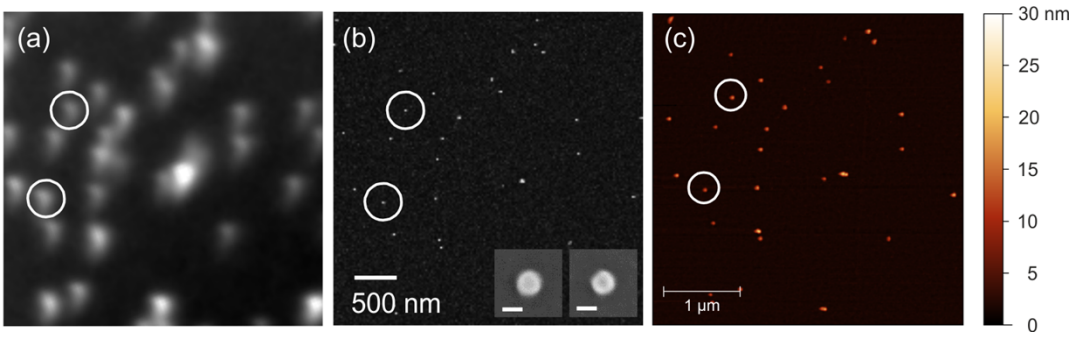

FIG. S1 (a) PEEM elemental contrast image, (b) SEM and (c) AFM images from the same area in the sample. The spots marked with circles correspond to single Fe nanoparticles with regular shapes, as shown in the high magnification SEM images [shown as insets in (b), with a scale bar 20 nm wide], which were selected for data analysis.

(ii) Simulation of x-ray absorption spectra (XAS) and magnetic contrast

The XAS spectra were simulated following the procedure described in Refs. [4,5]. Data for the energy dependent linear attenuation coefficients and the effective electron escape depth for the different materials were taken from Refs. [4,6]. To obtain the magnetic contrast at the Fe^0 L_3 edge, the simulations were carried out by including the magnetic circular dichroism effect (XMCD) of the different materials.[4,6] As discussed in the main text, a semi-infinite iron bulk system with two oxide layer with adjustable thickness is simulated, which provides a sufficient approximation when probing supported nanoparticles with the present sizes in PEEM. This procedure was carried out for the different oxygen exposures for which a full spectroscopic characterization was carried out, as discussed in the main text. From these fits, estimates for the different oxide layer thicknesses were obtained, and the evolution of the oxidation process is discussed in the main text. Here, we wish to illustrate the sensitivity of the fitting process to the presence of the different oxide layers, in particular by illustrating that by using both the magnetic and spectral information we are able to obtain reliable and accurate information about the presence of FeO-like and Fe_3O_4-like oxide layers, and their layer thicknesses.

In Fig. S2a we show first the simulated XAS spectra of a pure iron sample for the two circular light polarizations ($C^{\pm}$). The magnetization is set parallel to the x-rays, which impinge perpendicular to the surface, as illustrated in the inset to Fig. S2a. The magnetic contrast of a particle is simulated by calculating the normalized XMCD asymmetry from these spectra at the Fe^0 L_3 edge energy (dashed vertical lines in Fig. S2). The isotropic XAS spectra are calculated by averaging the XAS spectra with C^+ and C^-. The result is then scaled to match the

experimental data as shown for the pure iron sample in Fig. 4a. Oxidation will change the the XAS spectral shape as well as the normalized XMCD asymmetry. This is also seen in our simulations as demonstrated in Figure 2Sb, where 13 Å Fe_3O_4 (non-magnetic) and 5 Å FeO have been added on top of the magnetic iron in the simulation. Actually, we find that this layer stack reproduces *simultaneously* both the experimentally observed XAS and the reduced XMCD asymmetry at the Fe L_3 edge energy after 80 L oxygen dosage (cf. Fig. 4d and 4e). We may note that to compare the simulated XMCD asymmetry values quantitatively with the experimental data, one has to consider that the randomly oriented magnetization **m** of the particles will in general not coincide with the x-ray propagation direction **k**. Accordingly, the experimentally observed magnetic contrast is reduced when compared to the simulated case, where **m** and **k** are set parallel. This fact is taken into account by scaling *all* simulated XMCD asymmetries of a single particle with the *same* factor for the various oxide layer compositions.

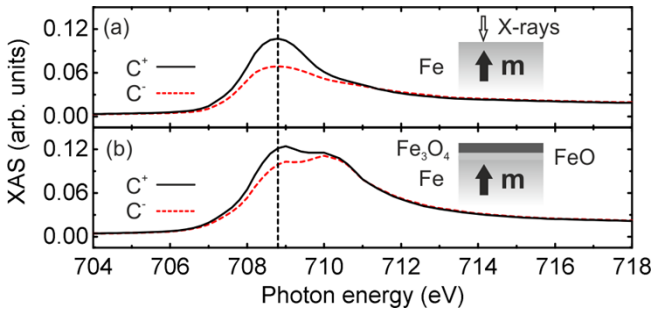

FIG. S2 (a) Simulated XAS spectra for (a) a semi-infinite iron sample for circularly polarized x-rays with opposite helicities $C^{\pm}$ and (b) for a semi-infinite iron sample capped with 13 Å non-magnetic Fe_3O_4 and 5 Å FeO. Insets show the schematic geometry for each case. In all simulations the x-rays are assumed to impinge normal to the surface.

For the present analysis, we require in all cases that the simulated isotropic XAS spectrum and XMCD asymmetry at the Fe^0 L_3 edge *simultaneously* match the experimental data at a given oxygen dosage. The results in Fig. 4 represent the best fits of the simulations to the present experimental data. In addition to the particular oxide thicknesses, good fits to the data require that the oxide layers are not magnetically polarised. This aspect is illustrated next.

(a) First, we demonstrate that we can exclude a ferrimagnetic Fe_3O_4 layer that couples ferromagnetic or antiferromagnetically to the iron core. For this purpose we consider the same stack as before (13 Å Fe_3O_4 and 5 Å FeO on top of iron), but assume a ferrimagnetic Fe_3O_4 layer instead of the non-magnetic Fe_3O_4. This stack would still reproduce the isotropic XAS spectra in Fig. 4d, but the magnetic contrast at the Fe L_3 edge energy would change due to the

XMCD effect of ferrimagnetic Fe_3O_4. Corresponding simulations are presented in Fig. S3. We find that a ferromagnetic coupling (Fig. S3a) would lead to an enhanced magnetic contrast at the Fe^0 L_3 edge, when compared to the simulations with a non-magnetic Fe_3O_4 layer. Quantitatively, we find that the XMCD asymmetry of this simulated layer stack is actually equal to the magnetic contrast of the pure metallic iron. In contrast, the experimental data show a reduction of about 50% of the XMCD asymmetry after exposure to 80 L oxygen, as shown in Fig. 4e. Considering under the same conditions an antiferromagnetic coupling of ferrimagnetically ordered Fe_3O_4 layer to the iron core leads to a cancellation of the XMCD effect at the Fe^0 L_3 edge in the simulations depicted in Fig. S3b, which is also in disagreement with the experimental observation.

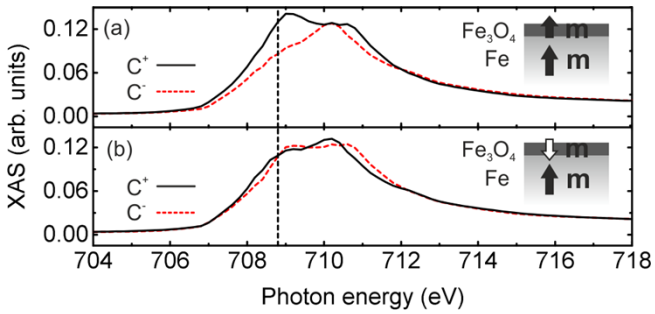

FIG. S3 (a) Simulated XAS spectra of a semi-infinite iron sample capped with 13 Å ferrimagnetic Fe_3O_4 and 5 Å FeO for circularly polarized x-rays with opposite helicities, $C^{\pm}$. Ferromagnetic coupling of the Fe_3O_4 layer to the iron is assumed as shown in the inset. (b) Simulated spectra as in (a), but with an antiferromagnetic coupling of the Fe_3O_4 layer.

(b) Our simulations show further that it is not possible to explain the experimentally observed reduction of the XMCD asymmetry without considering a FeO layer between the Fe and a non-magnetic Fe_3O_4 layer. Fig. S4a depicts simulated spectra for $C^{\pm}$-polarization for a single non-magnetic Fe_3O_4 layer with a thickness of 23 Å on top of the magnetic Fe. With this thickness it is possibe to reproduce the experimentally observed reduction of the XMCD asymmetry after 30 L oxygen dosage (cf. Fig. 4e). However, the simulated isotropic XAS spectrum (black line) in Fig. S4b reveals a significantly higher magnitude of the higher energy peak than what is found experimentally (circles in Fig. S4b and Fig. 4c, respectively), showing that a single, non-magnetic Fe_3O_4 layer cannot explain the experimentally observed magnetic contrast and the XAS simultaneously. A fit as displayed in Fig, 4c is only obtained when considering a stack of 8 Å Fe_3O_4 (non-magnetic) and 8 Å FeO on top of the magnetic metallic

iron. We may further note that varying the simulated layer thicknesses by about 2 Å leads already to noticeable disagreement with the experimental data.

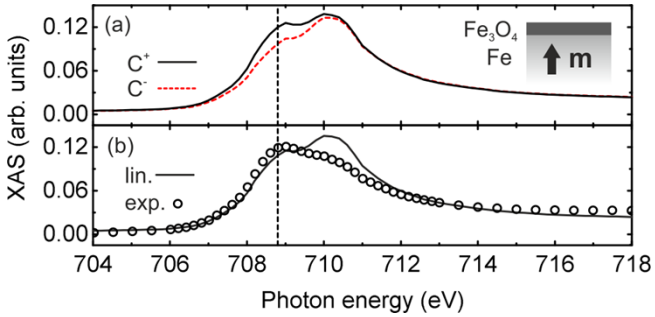

FIG. S4 (a) Simulated XAS spectra of a semi-infinite iron sample capped with 23 Å non-magnetic Fe_3O_4 for circularly polarized x-rays with opposite helicities $C^{\pm}$. The considered geometry is shown in the inset. The resulting XMCD asymmetry at the Fe^0 L_3 edge matches the experimental value after dosing 30 L oxygen. However, the simulated isotropic XAS spectrum (black line) in (b) clearly deviates from the experimental observation (circles), cf. Fig. 4c.

These examples illustrate the sensitivity of the simulated spectra to the exact experimental situation; the combination of both magnetic contrast information and full isotropic spectra, give strong constraints on the fits that enable the extraction of the oxide layer thickness with high confidence, despite the simplifications introduced by the model.

1 A. Fraile Rodríguez, A. Kleibert, J. Bansmann, and F. Nolting, *J. Phys. D: Appl. Phys*., 2010, **43**, 474006.

2 A. Balan, P. M. Derlet, A. Fraile Rodríguez, J. Bansmann, R. Yanes, U. Nowak, A. Kleibert, and F. Nolting, *Phys. Rev. Lett.*, 2014, **112**, 107201.

3 H. Hövel and I. Barke, *Prog. Surf. Sci.*, 2006, **81**, 53.

4 T. J. Regan, H. Ohldag, C. Stamm, F. Nolting, J. Lüning, J. Stöhr, and R. L. White, *Phys. Rev. B*, 2001, **64**, 214422.

5 R. Nakajima, J. Stöhr, and Y. U. Idzerda, *Phys. Rev. B*, 1999, **59**, 6421.

6 D. J. Huang, C. F. Chang, H.-T. Jeng, G. Y. Guo, H.-J. Lin, W. B. Wu, H. C. Ku, A. Fujimori, Y. Takahashi, and C. T. Chen, *Phys. Rev. Lett.*, 2004, **93**, 077204.